Toward Self-Assembly of Nanoparticles on Polymeric Microshells: Near-IR Release and Permeability

Matthieu F. Bédard,[†] Dieter Braun,[‡] Gleb B. Sukhorukov,[§] and Andre G. Skirtach[†,*]

[†]Max-Planck Institute of Colloids and Interfaces, Research Park Golm, Golm/Potsdam, D-14424 Germany, [‡]Center for Nanoscience, Ludwig Maximilian University of München, München, 80799 Germany, and [§]Department of Materials, Queen Mary University of London, Mile End Road, E1 4NS London, U.K.

ABSTRACT We present a novel approach to construct hollow polymeric microcontainers that can be remotely addressed using a low-power near-infrared laser to release encapsulated materials. Microshells possessing walls with aggregates of gold nanoparticles are found to release encapsulated materials upon near-IR irradiation, while shells containing the same amount of nonaggregated gold nanoparticles did not release their contents. The permeability of thermally shrunk microcapsules to dextran molecules is the lowest for shells containing nonaggregated nanoparticles and the highest for microcapsules with no nanoparticles. The wall thickness, roughness, influence of concentration of encapsulated materials, and general shrinking behavior of the microcapsules are studied. Aggregation of nanoparticles increases the absorption coefficient in the near-infrared part of electromagnetic spectrum. The temperature increase upon near-infrared laser illumination for different gold nanoparticle distributions is simulated. Important implications of this approach are expected in development of drug delivery systems as well as in temperature- and light-sensitive materials and membranes.

KEYWORDS: self-assembly · nanoparticles · microcapsules · aggregation · nanoassemblies · infrared light · temperature · polyelectrolyte multilayers

Controlling the distribution of nanoparticles is a key component of present and future technologies due to its applications in patterning and self-assembly.[1–7] The quantum properties at the surface of noble metal nanoparticles differ from that of their bulk material counterparts in terms of molecular interactions and electronic, optical, and magnetic properties.[8,9] A distinct feature of nanoparticles of noble metals is the presence of a surface plasmon resonance. The effects of symmetry are very important at the nanometer scale; for example, changing the size and shape of nanoparticles can influence their color. The surface of nanoparticles can be functionalized[10,11] or altered *via* chemistry,[12,13] making them quite versatile. In addition, noble metal nanoparticles have the ability to absorb light and convert it into thermal energy.[14–16]

Due to their high charge density, small size, and light absorption properties, nanoparticles are an ideal material to functionalize polyelectrolyte microcapsules, which were first introduced by Möhwald and co-workers in 1998.[17] The microcapsules or microshells are constructed *via* a technique known as layer-by-layer (LbL) assembly[18] in which oppositely charged polyelectrolytes are adsorbed onto sacrificial colloidal particles.[19,20] While encapsulation methods developed in recent years for polymeric microcapsules (such as the use of pH, ionic strength, heat, and light) cover many encapsulation needs, the development of release techniques tends to be much more challenging because they should not affect the capsule's load and host material.[21–25] The challenges of release of encapsulated materials transpire in applications in living tissues wherein mechanical and chemical release become unsuitable. To overcome this issue, a method for remotely releasing encapsulated material using laser light was recently introduced.[26,27] The release procedure discussed in this text takes advantage of the light-induced heat generation on gold nanoparticles (AuNPs), which is used to remotely trigger changes in the permeability of polymeric microcapsules. Other methods to remotely induce changes in microcapsules include enzymatic degradation and self-rupture,[28,29] release by magnetic fields and ultrasound,[30,31] and control of wall permeability by carbon dioxide.[32]

In biomedical applications of laser-induced remote release, it is desirable to obtain structures possessing near-IR absorption (NIR) that would alleviate potential side effects to biological tissue.[26] Gold nanorods have been used as efficient absorption centers in the NIR, and their wavelength-dependent absorption was recently studied.[33–35] However, the large concentration of stabilizers necessary for the synthesis and storage of these nanorods

*Address correspondence to skirtach@mpikg.mpg.de.

Received for review April 10, 2008 and accepted June 17, 2008.

Published online August 28, 2008.
10.1021/nn8002168 CCC: $40.75

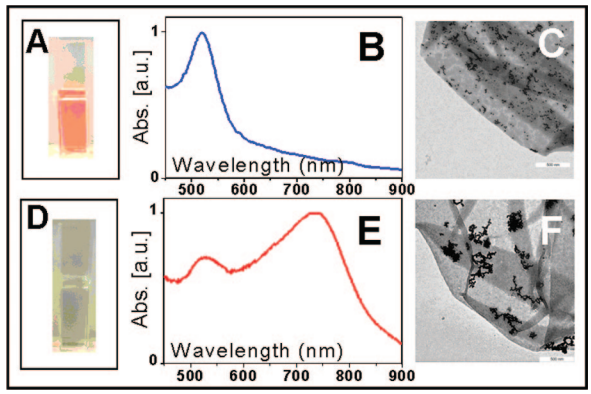

Figure 1. A solution of citrate-stabilized gold nanoparticles has a red color as seen through a plastic cuvette (A). Its corresponding UV/visible absorbance spectrum shows a strong absorbance peak at 520 nm (B), and TEM image of dry (PDADMAC/Au/PSS)$_4$ shells with nonaggregated gold particles (C). The color of the gold solution after adding salt is blue/gray (D), its corresponding absorption spectrum (E), and the general appearance of these aggregates as seen when inserted in the wall of (PDADMAC/Au/PSS)$_4$ microcapsule (F). Scale bars in TEM images correspond to 500 nm.

affects their interaction with other materials. An alternative approach offering NIR absorption is possible by aggregating metallic nanoparticles.[36,37] Although there has been some work that studied the nature of the aggregation process of AuNPs, applications of such assemblies of nanoparticles in complex systems have been limited.[38] In regard to polymeric microcapsules, another potential advantage of aggregating the particles lays in the possibility to concentrate or localize the heat generation potential of AuNPs, maximizing the efficiency of the light-induced release. In our previous work, we focused on controlling the distribution of nanoparticles at high concentration on polyelectrolyte multilayers.[39] In this work, we present the general influence and potential benefits changing the distribution of AuNPs within the shell of polyelectrolyte microcapsules on capsule properties such as thermal stability, permeability, as well as encapsulation and release. In this regard, controlling the distribution of nanoparticles within the walls of polyelectrolyte microcapsules constitutes a great step toward self-assembly of nanomaterials.[40]

RESULTS AND DISCUSSION

Spectroscopic Properties of AuNPs. Aggregation in a stable solution of AuNPs by addition of electrolytes is visible by eye since a drastic color change from ruby/red to blue/gray results in the process (Figure 1A,D). The typical absorption spectra ($\lambda_{max} \sim 520$ nm) of a solution of citrate-stabilized AuNPs (average diameter $=$ 20 nm) are shown in Figure 1B. Citrate molecules added as a coordinating agent during the preparation of AuNPs prevent the latter from aggregating with each other through electrostatic stabilization. Flocculation of the AuNPs in solution may occur when the stabilizing charges of the citrate molecules covering the gold are compensated by a sufficient number of oppositely charged ions that lowers the long-range electrostatic repulsions and allows short-range attractive forces to (van der Waals forces) dominate.[37,41] After mixing (1:1) a solution of NaCl (0.1 M) with a solution of citrate-stabilized AuNPs (20 nm), the latter become unstable and the solution rapidly changes color as aggregation proceeds. The corresponding absorption spectrum displays a novel broad absorption region between 700 and 900 nm with a maximum centered at 740 nm (Figure 1E). A similar absorption peak, red-shifted by 20−30 nm, appears upon mixing a solution of potassium chloride (0.1 M) with an equivalent volume of AuNPs solution, but no IR absorbance peak appeared when mixing the gold solution with an equivalent volume of lithium chloride solution (0.1 M). No significant change in the absorbance spectra of AuNPs of diameters of 5 or 10 nm was observed when salt was added. Besides the appearance of a large absorption peak in the NIR, the addition of NaCl to the gold particle solution leads to a minor bathochromic shift of its surface plasmon resonance (SPR) band from 521 to 526 nm. In earlier work, we inserted AuNPs in the shell of polymeric microcapsules and used them to convert light into heat to rupture the microcapsules and release encapsulated material.[26,42] We note that the formation of aggregates of AuNPs (at high concentrations) on polyelectrolyte microcapsules was previously demonstrated,[39] but their response to irradiation, permeability, and surface roughness has not been investigated.

To form aggregates of AuNPs and insert them in the microcapsule wall, equal volumes of a solution of NaCl (0.1 M) and a solution of AuNPs (20 nm) were first mixed. After 60 s, the salt/AuNPs solution was used to resuspend a solution of silica particles coated with PDADMAC as the outermost layer. At the end of the shell assembly, the coated silica particles were treated with hydrofluoric acid (0.3 M) and thoroughly rinsed with water to remove the acid. Hollow capsules with an average diameter of 4.8 μm and possessing the following shell structure were obtained: (PDADMAC/Au/PSS)$_4$. Citrate-stabilized AuNPs were added directly to the polymer-coated silica to form microcapsules with nonaggregated AuNPs, as shown by transmission electron microscopy (TEM, Figure 1C). In sharp contrast, TEM images of capsules assembled in the presence of NaCl aggregated AuNPs show that the polymeric shells obtained after treating the particles four times (after each PDADMAC layer addition) contain only aggregates of AuNPs (Figure 1F). The same concentration of AuNPs was used for the construction of microshells containing aggregated and nonaggregated nanoparticles. (It can be seen from Figure 1C that small aggregates appear to coexist together with single particles. Such slight aggregation appears when AuNPs are distributed over several polyelectrolyte layers but lack the change in absorbance found in shells assembled in the

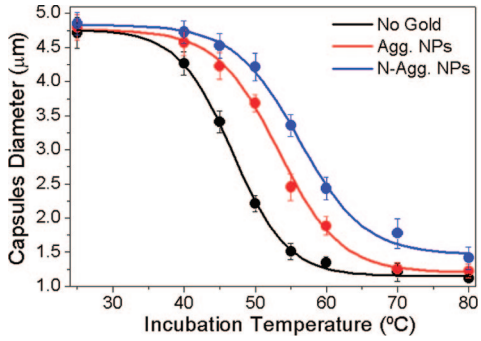

Figure 2. Heat shrinking behavior of $(PDADMAC/Au/PSS)_4$ microcapsules containing no gold particles, as well as aggregated and nonaggregated gold nanoparticles as a function of the incubation temperature. The diameter of 60 capsules was measured for each data point.

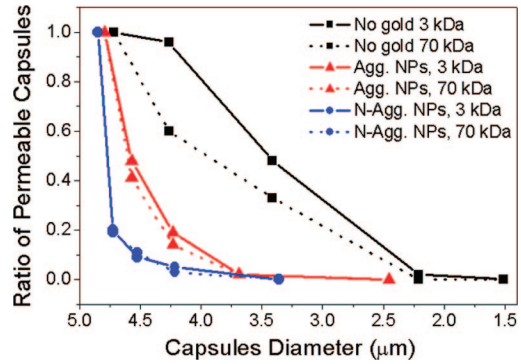

Figure 3. Relative permeability of microcapsules containing no gold (black), aggregated (red), and nonaggregated gold nanoparticles (blue) as a function of microcapsule's diameter. Polymeric shells were thermally shrunk to different sizes in the range of temperatures from 35 to 55 °C and at 5 °C intervals (data points from left to right). Shrunk capsules were then separately mixed with 3 or 70 kDa fluorescently labeled dextran molecules. The ratios of permeable capsules were determined from LSCM by measuring the fluorescence profiles of 60 capsules per data point.

presence of salt.) The supernatant taken out after each AuNP adsorption step was found to contain trace amounts of gold, corresponding to less than 1% of the amount of gold added; this indicates that all AuNPs added during the polyelectrolyte shell assembly adsorb to and remain in the capsules' walls.

Response of AuNP—Microcapsules to Thermal Shrinkage. Heating $(PDADMAC/PSS)_n$ microcapsules has been shown to induce the reorganization of loosely arranged polyelectrolyte layers into a denser structure.[43] Köhler and co-workers explained this effect as the result of exceeding the glass transition of the polyelectrolyte complex, which turns the layers into a viscoelastic state and reorganizes them driven by electrostatic and hydrophobic forces toward a state with lower total Gibb's energy.[44] Two other competing forces also exist during capsule shrinkage: the electrostatic and hydrophobic forces, which act outward and inward, respectively, relative to the capsule interior.[45] Thermally increasing the entropy incites more efficient, stronger electrostatic interactions between the oppositely charged layers (*i.e.*, enthalpy increase), accompanied by densification of the polymeric shell and subsequent reduction of its inner volume. Shrinking behavior can be adjusted by the total number of bilayers, while its direction is predetermined by an odd (swelling) or even (shrinking) layer number.[46] While denser microshells tend to be more mechanically stable, their permeability decreases with increasing bilayer number. We note that a side effect of inserting AuNPs within the wall of the microshell is to mimic the effect of increasing the number of layers without effectively changing their permeability before heat treatment. The thermal shrinking behavior of capsules containing aggregated, nonaggregated, and no AuNPs was studied. Figure 2 displays the heat shrinking behavior of the three shell types. It can be seen that, within the temperature range at which capsules shrink to diameters between 4.0 and 2.0 μm, microshells containing AuNPs needed higher temperatures to shrink to the same diameter compared with those containing no gold: shells containing nonaggregated AuNPs needed about 12 °C and those with aggregated AuNPs 7 °C. With an average size of 20 nm, the AuNPs used in this work are comparable to the wall thickness of microcapsules (measured by AFM: 19.2 nm (±1.6)) and are expected to slow down the shrinking of the polymeric shell during heating. However, from Figure 2, one finds that, at least in the case of capsules with nonaggregated particles, the minimal diameter to which the capsules can be shrunk to is also higher in comparison to the other two types of capsules. This suggests that during heating the decreasing surface area brings neighboring AuNPs in the microcapsule wall closer to one another so that they inhibit further shell shrinkage (*i.e.*, Percolation). One would expect a shell containing more particles or homogeneously distributed particles to be more affected by interparticle effects since encounters between particles are expected be more frequent than those in a microshell containing AuNPs with larger interparticle distances.

Permeability and Encapsulation Studies. In the previous section, we have shown that incorporating AuNPs in the walls of capsules changes their shrinking behavior; here we look into their permeability. Microcapsules were mixed with a solution of fluorescently labeled dextran of desired molecular weight for several minutes and then heated in a water bath for 20 min.[44,46] The solutions of shrunk microcapsules and dextran (MW = 3 or 70 kDa) were then stored in darkness for 24 h. The permeability of different microshells was measured by monitoring the diffusion of the fluorescent dextran to the cavity of microcapsules thermally shrunk to various diameters. The sample mixture was then deposited onto a glass slide and probed by LSCM for "leakiness". The results are shown in Figure 3. The fluorescence profiles of 60 capsules per data point were measured. A given capsule was considered permeable when, after the incubation period, its inner fluorescence was at

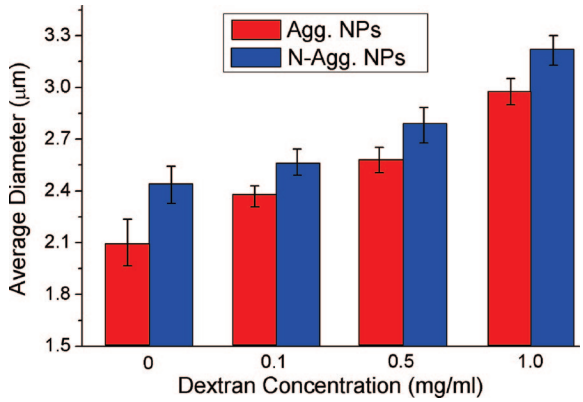

Figure 4. Influence of the concentration of fluorescently labeled dextran on the diameter of polymeric microcapsules. Microcapsules doped with aggregated and nonaggregated gold nanoparticles were thermally shrunk at 60 °C for 20 min in the presence of dextran concentration from 0.1 to 1.0 mg/mL. The diameters were averaged from confocal microscopy measurements of 20 shells for each data point.

least 50% that of the surrounding medium. It was found that, at comparable diameters, the effective permeability of thermally shrunk microshells doped with AuNPs is very different than the permeability of control samples containing no nanoparticles. In the vast majority of cases, the hollow capsules were found to contain no fluorescence (permeability ratio = 0) or the same fluorescence as the surrounding medium (permeability ratio = 1). With the exception of capsules that were not shrunk, the permeability of capsules to fluorescent molecules of either molecular weight is greater for capsules containing no gold and lesser for capsules containing nonaggregated AuNPs. As expected, 70 kDa dextran permeated the polymeric wall somewhat less efficiently than 3 kDa dextran, and this effect was observed in all samples. This information becomes particularly useful because together with the thermal shrinking behavior it provides the basis of encapsulation for various wall/nanoparticle compositions.

It is generally understood that heat shrinking of microcapsules increases the concentration of the encapsulated material (encapsulate) relative to the bulk concentration since the encapsulated molecules are confined to a smaller volume. The microcapsule wall acts as a semipermeable membrane of low permeability to large molecules but high permeability to water molecules so that osmotic effects can be neglected. As a result of the concentration difference of encapsulate across the capsule wall, a diffusive force arises upon shrinking the capsules to lower diameters. This diffusive force opposes the capsule shrinking to a certain extent and should increase with higher concentration of encapsulate. To find out if the encapsulate concentration has an effect on the thermal shrinking behavior of microcapsules, samples of capsules containing aggregated and nonaggregated AuNPs were heated at 60 °C in the presence of different concentrations of fluorescently labeled dextran (MW = 10 kDa). The samples were then washed with water to remove the nonencapsulated dextran. The average diameters of the microcapsules (≤20) thermally shrunk in the presence of 0.1, 0.5, and 1.0 mg/mL labeled dextran are presented in Figure 4. It was found that both types of microcapsules shrink less with increasing concentration of dextran. It is expected that encapsulating higher concentrations of material could limit the shrinking process to a point where no encapsulation takes place since the capsules' walls would be unable to become dense enough to prevent leakage. Therefore, the behavior observed in Figure 4 is consistent with the assumption that a diffusive force is generated by the dextran as the volume of the shell is decreased. Furthermore, the capsule shells were found to remain nonfluorescent after being added to a solution of labeled dextran molecules and subsequently washed, supporting diffusion through the capsule's wall; the uncharged dextran does not bind to the polyelectrolyte's shell and therefore is not expected to interfere with the shrinking process.

On the basis of the variations in thermal shrinkage and permeability discussed so far, we hypothesized that these changes may be the result of an influence of the AuNPs over shell thickness. If this were true, the shell of samples containing nonaggregated AuNPs would be expected to possess more polyelectrolyte material or a denser structure. A change in overall shell density directly due to the presence of nanoparticles is unlikely due to two facts: first, the permeability of the different capsules would differ before heating, and second, the shells contain a relatively low gold content that should have no consequence over the shell areas containing no nanoparticles. The latter point will be discussed at the end of this section. The thickness of capsules before and after a brief period of thermal shrinking was measured by AFM (from the areas containing no gold nanoparticles; Table 1). Before shrinkage, the

TABLE 1. Shell Thickness[a] of Different $(PDADMAC/PSS)_4$ Capsules Containing Aggregated and Nonaggregated Gold Nanoparticles, as well as a Control (without Nanoparticles), before (before T), and after (after T) Thermal Shrinking to Similar Diameters

	control		aggregated NPs		nonaggregated NPs	
	diameter (μm)	thickness (nm)	diameter (μm)	thickness (nm)	diameter (μm)	thickness (nm)
before T	4.9 ± 0.3	19.4 ± 1.1	4.8 ± 0.2	19.2 ± 1.5	4.9 ± 0.3	19.5 ± 1.2
after T	4.5 ± 0.2	20.6 ± 0.8	4.4 ± 0.3	23.2 ± 0.9	4.4 ± 0.3	30.1 ± 0.8

[a] Statistical measurements were calculated from the average thickness of 30 capsules.

average shell thicknesses of control capsules with no gold and those with nonaggregated and aggregated AuNPs were 19.4 ± 1.1, 19.2 ± 1.5, and 19.5 ± 1.2 nm, respectively. No significant difference in the wall thickness was found between the three capsules types. This is consistent with our observation in Figure 3 that the microcapsules were all equally permeable to two different dextran sizes before heating. Samples of each microcapsule solution were then thermally treated to verify our aforementioned hypothesis. For capsules that were shrunk, the average shell thicknesses of the control and aggregated AuNP samples were found to increase by 6 and 17%, respectively. A surprisingly large change in the wall thickness of *ca.* 35% was measured for microshells containing nonaggregated AuNPs. The shrinking temperatures were selected from Figure 2 in order to obtain all microcapsules of approximately 4.4 μm in diameter (90% of their original diameter)—the size at which a significant difference in permeability occurs, as illustrated in Figure 3.

During capsule assembly, the polymeric material that precipitates onto silica particles does so in the glassy state and becomes tightly bound to the oppositely charged layer. In solution, the positively charged PDADMAC-coated silica particles absorb all of the negatively charged AuNPs added. The latter remain electrostatically attached to the PDADMAC layer despite centrifugation and several washings in water as indicated by the absence of color in the supernatants. Since the AuNPs used have a diameter comparable to the final shell thickness, we can postulate that significant quantities of polyelectrolyte material absorb around the AuNPs. The absorption of polyelectrolytes around AuNPs and their subsequent insertion in polymeric shells was discussed in previous work.[39] The surface filling factor (F_S),[47] a measure of the ratio of the total area covered by nanoparticles per capsules, to the surface area of the capsules was calculated to be 0.05 for microshells containing nonaggregated AuNPs used for the permeability studies (Figure 3). In other words, about 5% of the total area of the capsules containing nonaggregated particles is covered by gold. For this reason, the mere presence of nanoparticles cannot be the sole reason for the permeability changes observed.[47] Instead, we have to consider that a spherical 20 nm AuNP has a considerably larger surface area than the planar surface of the microcapsule it spans. We assumed that some of the material absorbed around AuNPs could potentially diffuse in the nanoparticle's periphery during thermal treatment, making shell regions between AuNPs thicker/denser, leading to a change in wall permeability. To verify the validity of this argument, we looked for indications that the roughness of the shells changes during thermal treatment using AFM. Figure 5 illustrates the roughness differences between microcapsules doped with nonaggregated (A,B) and aggregated (C,D) AuNPs, before (A,C) and after (B,D) thermal treatment. In each image, the position of some AuNPs is indicated with an arrow. The surface of heated microcapsules was found to become much smoother and, generally, the shape of AuNPs became better defined (see Supporting Figure 1). This second observation suggests that a thinning of the material coating the nanoparticles occurs during heating and that this material was most likely redistributed in shell areas around the nanoparticles. Comparison of panels A and C of Figure 5 shows that capsules containing nonaggregated AuNPs are much rougher than those doped with aggregates. It follows that, during LbL assembly of the microcapsules, a rougher surface comes with more surface area available for subsequent layers to adhere. Since the aggregates found in the samples consist of a dozen to hundreds of particles, much of the gold surface is occupied by adjacent particles within the aggregate. The differences in the thickness of microcapsules containing aggregated and nonaggregated AuNPs that were discussed in Table 1 support this argument. It should be noted that the large roughness of the capsules, combined with the presence of folds and the different distribution of nanoparticles of these samples, made it impossible to compare sample roughness quantitatively.

Mueller and co-workers showed that, at high temperatures, the shell components of PDADMAC/PSS capsules switch from a glassy to viscoelastic state, a phenomenon accompanied by a reduction in the wall surface tension and corresponding tendency of the capsule wall to reduce its surface area.[48] Surface tension effects account for the tendency of shell material to diffuse around the shell at temperatures above T_g. At elevated temperature ($T \uparrow$), polymeric material that covers the AuNPs melts and diffuses to lower areas in order to reduce the surface area of the shell that is exposed to water—a surface tension effect. After cooling, the now thicker/denser interparticle regions of the shell are less permeable to the same molecule. Figure 6 summarizes our general hypothesis, showing a cross-section of a shell containing two embedded AuNPs that is permeable to a molecule.

Encapsulation and NIR-Induced Release of Dextran. Microcapsules with the shell structure $(PDADMAC/Au/PSS)_4$ were used to compare the release efficiency of shells containing nonaggregated and aggregated AuNPs. For the laser-induced release experiments, fluorescently labeled dextran was encapsulated at 54 and 59 °C for capsules doped with aggregated and nonaggregated AuNPs, respectively. These temperatures were chosen from the data plotted in Figure 2, to obtain samples of comparable diameter, wall thickness, and fluorescence intensity. In accordance with the data obtained from the permeability studies, the samples retained the encapsulated material and no changes in fluorescence intensity were found after 5 months of storage (4 °C, dark conditions). $(PDADMAC/Au/PSS)_4$ microshells with

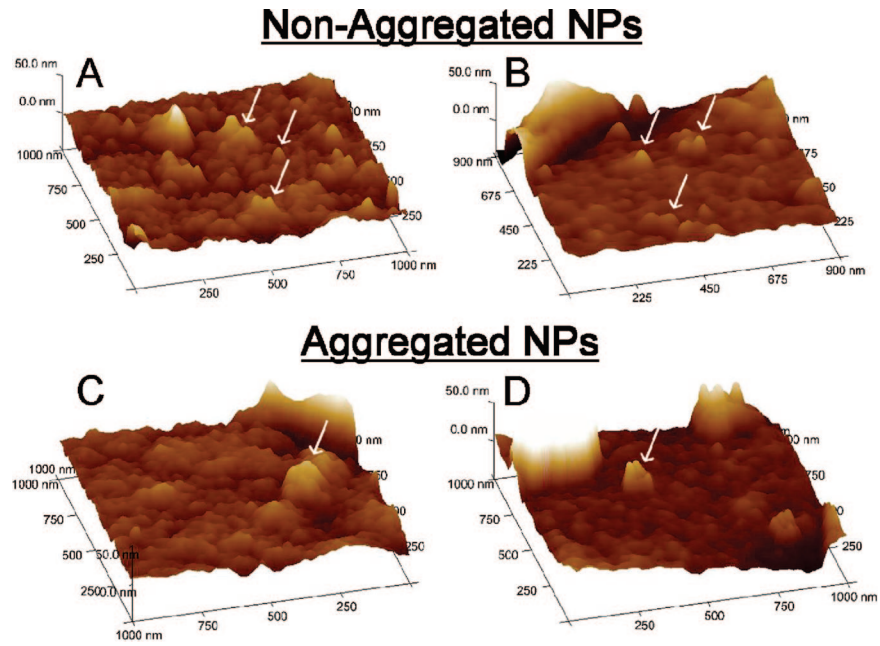

Figure 5. AFM visualization of the changes in the surface roughness of capsules. Top: 3D representation of the surface profiles of capsules doped with nonaggregated gold nanoparticles before (A) and after heating at 40 °C for 20 min (B). Below: Capsules containing aggregates of gold nanoparticles before (C) and after heating (D). Some single particles (A,B) and aggregates (C,D) are indicated by an arrow in the images. Nonaggregated gold nanoparticles render the capsule's surface very rough in comparison to capsules containing aggregated particles. The roughness of either type of capsules is decreased to a similar degree after heating (if the larger aggregates are excluded from roughness measurements). Areas shown corresponds to 0.9−1 μm^2. The height scale is 50 nm.

encapsulated dextran were then irradiated using the laser setup reported in earlier work.[47] Thirty capsules were irradiated in each experiment. The release of encapsulated materials from the microcontainers containing nonaggregated and aggregated AuNPs was remarkably different. In the former case, none of the microcapsules exposed to the laser beam could be opened (Figure 7A,B) within the whole range of incident laser powers (1−90 mW), also indicating that no photobleaching takes place. The fluorescence of laser-irradiated unopened microcapsules did not change after 48 h. A graph plotted using the percentage of open capsules as a function of laser intensity gives a flat line (Figure 7C). In sharp contrast, the dextran content encapsulated in microcapsules with aggregated nanoparticles was entirely released at about 70 mW. In Figure 7D, each capsule was irradiated with the infrared laser for 5 s at 65 mW and was subsequently opened as pictured in Figure 7E. The capsule that remains fluorescent after irradiation was deliberately kept away from the laser to demonstrate that the fluorescence intensity of the capsules did not change after the irradiation of proximal capsules. The percentage of microcapsules optically opened in this manner decreased at lower intensity as illustrated in Figure 7F (solid line). The minimum laser power required to remotely open capsules containing aggregated AuNPs was found to be *ca.* 10 mW. At intensities below 60 mW, a second laser exposure of 10 s was performed on microshells that were not open in the first experiment. We observed that up to 12% more capsules could be opened after the second irradiation trial. Repeating the irradiation procedure more than twice or increasing the time of irradiation above 10 s did not further improve the ratio of opened/closed capsules, at any given intensity. A derivative plot of the data points found in Figure 7F (solid line) was obtained (dashed line). The peak of this curve, centered at 36 mW, is referred to as the threshold intensity (TI). TI is defined as the intensity necessary to open more than 50% of capsules.

The moderately broad range of laser intensities required to open capsules (*ca.* 60 mW) can be partially attributed to the size of AuNP assemblies sandwiched within the shell. The LSCM images D,E in Figure 7 demonstrate that upon irradiation the capsules released their fluorescent content entirely. In addition, the laser-induced release of material from microcapsules observed in LSCM was never accompanied by their deformation or "explosion" which was observed in the previous work[42,47] and which may limit applications due to potential damages to encapsulated materials and surrounding.

In order to explain the influence of different arrangements of AuNPs on laser-induced release behavior, we first need to consider the spectroscopic changes found in aggregated nanoparticles. The near-IR absorption of the aggregates of AuNPs originates from the interaction of dipole moments of two or more AuNPs. The broadness of the NIR absorption peak presented in Figure 1E supports the fact that after adding salt the formed AuNP assemblies have a large size distribution. The

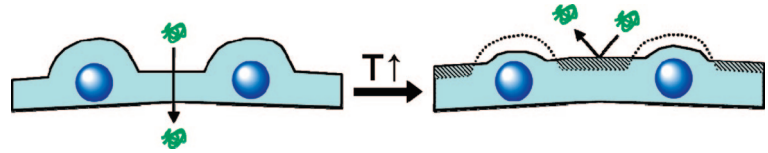

Figure 6. Cross-sectional representation of a PDADMAC/PSS multilayer containing gold nanoparticles before and after thermal treatment. Left: Interparticle regions of the wall are originally permeable to a molecule before heating. Right: During thermal treatment, surface tension effects force the excess polyelectrolyte material surrounding gold particles to contribute to the interparticle wall thickness, decreasing the shell permeability.

number of particles per aggregates in capsules was estimated by TEM and found to vary largely, from roughly 15 to about 100 particles per assembly. Dynamic light scattering (DLS) was used to attempt to monitor the average size of AuNP assemblies (by mass) as a function of time (see Supporting Figure 2), but each measurement needed about 60 s and most of the aggregation process occurs within this time period. In some instances, we observed that incorporating larger aggregates containing more than 300 AuNPs brings about defects to the microshells and renders encapsulation less efficient. The main criterion to partially control the size of the aggregates of citrate-stabilized AuNPs appears to be the duration of incubation of AuNPs with salt. It was also demonstrated that stirring velocity, the order, and rate of the mixing the electrolyte and gold solutions may also have a great influence over the aggregation behavior.[41] The second point that should be considered to explain the high release efficiency of capsules containing aggregates of AuNPs concerns the localization of the particles over a small area of the microcapsule wall. Microcapsules containing nonaggregated AuNPs require relatively intense laser irradiation, which, in turn, is more likely to induce irreversible damages to the shell, its content, and host material (*e.g.*, living tissue, cell).[42] Concentrating the particles to a smaller volume within a capsule shell leads to a localization of the heat produced by the nanoparticles upon light absorption. Therefore, aggregating AuNPs increases the surface-to-volume ratio of the IR absorbing nanoparticles, inducing the temperature of the shell material surrounding the absorption centers to rise and accumulate in a larger area. In this sense, using nonaggregated particles has the double disadvantage of not absorbing much in the IR range and having to absorb much more light to produce enough heat to melt sufficiently thick regions of polyelectrolyte complex so that a change in wall permeability can occur. A milder temperature increase around an aggregate of AuNPs, sufficient to exceed the glass transition (T_g) of the surrounding polyelectrolytes within the capsules' shell, should be plausible. Being less dense above T_g, molten regions of the capsule shell then become more permeable, allowing encapsulated material to leak out (or solution components to flow in). The individual T_g value of PDADMAC (70 °C) and PSS (200 °C) significantly decreased in an aqueous environment.[49,50] Using differential scanning calorimetry (micro-DSC), we previously determined that $(PDADMAC/PSS)_4$ shells in water possess an endothermic peak centered at 40 °C, with an onset situated at 35 °C.[44] Taking into account that experiments were done at an ambient temperature of 25 °C and assuming that T_g for $(PDADMAC/Au/PSS)_4$ capsules does not vary significantly from that of $(PDADMAC/PSS)_4$ shells, it is highly probable that an increase of 10 °C or more is necessary to exceed T_g.

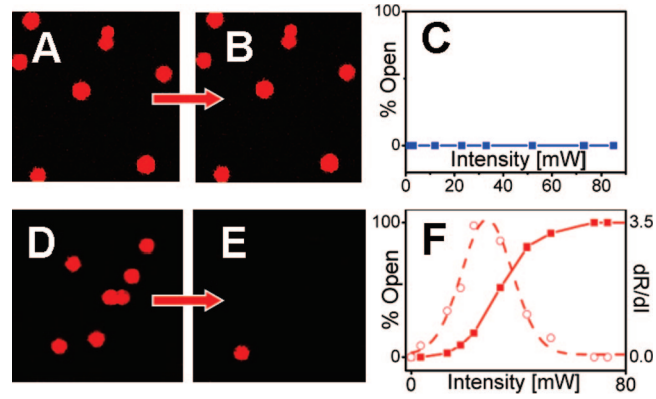

Figure 7. (Top) Capsules containing nonaggregated gold particles: representative LSCM caption of microcapsules with encapsulated Alexa Fluor 555 dextran before (A) and after (B) exposure to infrared laser. No capsules could be opened at any power intensity (C). (Bottom) Capsules with aggregated gold particles: microcapsules with encapsulated labeled dextran before (D) and after (E) exposure to infrared laser using an incident intensity of 65 mW. A plot correlating the % of capsules opened (30 capsules per measurement) as a function of power (F, solid line) and its derivative (F, dashed line) are shown.

Simulating the Heat Distribution around Nanoparticle Assemblies. The release of encapsulated polymer upon NIR laser illumination from microcapsules containing aggregated nanoparticles is due to their higher absorption of laser light. We have simulated the temperature rise on nonaggregated and also on aggregated AuNPs. The size of nanoparticles taken was 20 nm, the absorption coefficient[39,51] of nanoparticles, Q, is ~1.6 at the surface plasmon resonance (520 nm) and $Q \sim 0.02$ at 830 nm. Using these parameters, the temperature rise on a single AuNP was calculated to be ~0.5 K when illuminated at 830 nm with a power of 50 mW. In the simplest aggregation case, where a short linear chain of AuNPs is formed, a second absorption peak can be found in the NIR region of the electromagnetic spectrum. The absorption coefficient at 830 nm for an aggregate of AuNPs is estimated to increase 5-fold ($Q \sim 0.1$) in comparison with stand alone nanoparticles.[36] In addition, another effect that contributes to temperature rise upon aggregation is surface-to-volume ratio upon bringing nanoparticles in close proximity, which was estimated to contribute up to 30% of the temperature rise. The temperature increase presented in Figure 8 was adjusted due to absorption change of aggregation, and although a single nanoparticle was calculated to increase its immediate environment by less than 1 K, a linear assembly of four nanoparticles can produce up to 7 K. If a small aggregate composed of merely four AuNPs already has the potential to produce a significant temperature rise, then the larger and more complex aggregates induce larger temperature rises. Examples of a nonaggregated and linear assembly type of AuNP distribution in microshells are shown in panels A and B of Figure 8, respectively. The microcapsules used for this work were found to possess aggregates containing between a dozen to over a hundred AuNPs

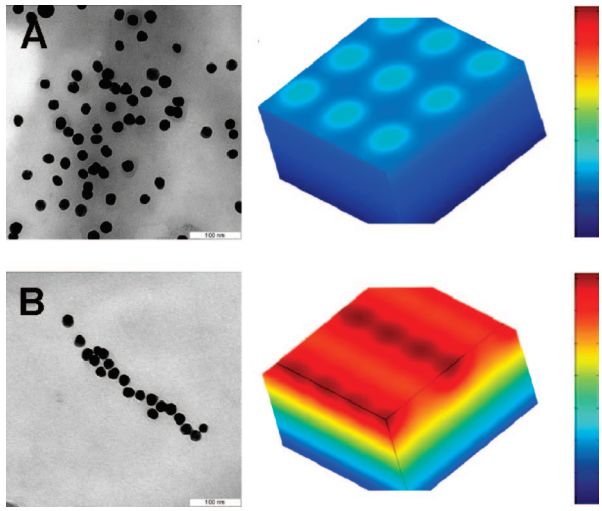

Figure 8. Modeling the temperature distribution for nonaggregated (top) and aggregated nanoparticles (bottom). Nonaggregated nanoparticles do not possess absorption in the near-IR part of the spectrum. For 20 nm nanoparticles, the absorption coefficient is about 0.02 at 830 nm, so the temperature rise at 50 mW of incident power is less than 1 degree. For a single line of four aggregated nanoparticles, a temperature rise of 7 K can be produced (red). TEM images of uniform distribution and aggregates of nanoparticles are shown on the left side of corresponding simulations. The scale bars for the TEM images are 100 nm.

assembled in linear or mesh-like aggregates. We suspect the larger, more common mesh-like type of nanoparticle assembly to be the result of several linear structures aggregating together. Larger aggregates are expected to produce even higher temperature rises than estimated here due to higher surface-to-volume ratio. The temperature rise on a linear aggregate is illustrated in the simulation, Figure 8B, where the heat produced by the centermost linear structure appears to overlap with that of a second nearby assembly (and there is no blue or cooler region in between). On the other hand, the nonaggregated nanoparticles do not induce substantial temperature rise (Figure 8A). As noted above, the closely located nanoparticles increase temperature due to higher surface-to-volume ratio and interacting dipole moments induced on each nanoparticle. Our data for estimating the temperature rise are in agreement with those published by other groups,[52] and we note that the temperature rise is not sufficient for vapor bubble formation[53] and cell destruction.[54]

CONCLUSIONS

Polyelectrolyte PDADMAC and PSS hollow shells were constructed and functionalized with citrate-stabilized gold nanoparticles in either uniform (nonaggregated) or aggregated (possessing near-IR peak) state. For encapsulation by thermal shrinking, microcapsules with nonaggregated gold nanoparticles require more thermal energy than those with aggregates, while both types require higher temperatures than the control sample containing no nanoparticles. This behavior is ascribed to the limitations in lateral movement of polymers upon introduction of nanoparticles. In the thermally shrunk state, the permeability of the microshells to dextran polymers is the highest for microcapsules possessing no nanoparticles, while it is the lowest for microcapsules with uniform distribution of nanoparticles. This is attributed to the wall of the microshells becoming thicker or denser at elevated temperatures as a result of additional polymeric material that formed multilayers around the gold particles diffusing between neighboring gold particles. The shrinking of polymeric microshells doped with both nonaggregated and aggregated gold nanoparticles depends on the concentration of encapsulated dextran molecules. Release of the encapsulated materials from capsules containing aggregates of gold particles can be performed at low power of near-IR laser, while no release takes place for capsules containing nonaggregated gold particles. This difference is explained by more efficient, localized temperature rise around aggregates of gold nanoparticles due to higher absorption coefficient and higher surface-to-volume ratio—calculations of the temperature rise agree well with these conclusions. The results presented in this work are relevant for intracellular delivery,[26] membranes,[55] nanoparticles delivery,[56] anticorrosion protection,[57] and other light- and thermo-responsive materials and methods in general.

METHODS

Preparation of Silica Templates. The fabrication of (PDADMAC/Au/PSS)$_4$ microcapsules was done on 4.78 μm (Microparticles GmbH, Germany) particles using the layer-by-layer deposition technique. Typically, 1 mL of template SiO_2 particles solution was first cleaned from stabilizers in a sonication bath after resuspending them in a 1:1 solution of water and isopropanol.

Layer-by-Layer Assembly of Polyelectrolyte Microshells. Solutions of poly(diallyldimethylammonium chloride) (PDADMAC, Sigma-Aldrich) (2 mg/mL, 0.5 M NaCl), 20 nm colloidal gold (Sigma-Aldrich), and poly(styrenesulfonate, sodium salt) (PSS, Sigma-Aldrich) (2 mg/mL, 0.5 M NaCl) were prepared without further purification. For the capsule sample containing nonaggregated gold nanoparticles, SiO_2 templates with PDADMAC as the outermost layer were resuspended in a mixture of water and colloid gold solution while gently stirring. For microcapsules with aggregates of nanoparticles, the same mixture of colloidal gold was prepared but in a solution of 0.1 M NaCl and was left to incubate for 60 s before resuspending the PDADMAC-coated silica with the solution of now aggregated gold. The templates were further dissolved in HF (0.3 M) solution, and the sample was then washed with water until the pH of the solution reached >5.

Thermal Shrinking of Microshells, Permeability, and Encapsulation of Fluorescently Labeled Polymer. General thermal shrinking behavior was determined at 5−10 °C intervals from 30 to 80 °C by immersing a microcapsule suspension in a thermostatted water bath for 20 min. Capsule diameter and standard deviation (CL = 95%) were determined by averaging the diameter of 30 capsules using a laser scanning confocal microscope. The permeability ratios of microshells as a function of shell diameter were determined from profiles of 60 capsules per data point. Polymeric shells were thermally shrunk to different diameters from 35 to

55 at 5 °C intervals. After cooling, the shrunk samples were separated in two aliquots, each mixed with either Alexa Fluor 488 dextran (AF488, 3 kDa, Invitrogen, Germany) or TRITC dextran (65−76 kDa, Invitrogen, Germany). The encapsulation of Alexa Fluor 555 dextran (AF555, 10 kDa, Invitrogen, Germany) was done by heating a mixture of capsules and AF555 (0.1 mg/mL) for 20 min at required temperatures. For remote release experiments, shrinking was done at 54 and 59 °C for samples containing aggregated and nonaggregated gold, respectively. The mixture was left to vortex at low speed for 20 min before heating in order to allow the fluorescent polymer to diffuse across the multilayer complex. The samples were allowed to cool for 5 min and washed twice with water to remove nonencapsulated fluorescent label.

Microshell Characterization. Transmission electron microscopy (TEM) was done using a Zeiss Omega EM 912 at an operating voltage of 120 kV. Confocal laser scanning microscopy (CLSM) was used to visualize the capsules in solution. Images were recorded by means of a 100×/1.4−0.7 oil immersion objective. A CARY 50 conc. (Varian, Germany) UV−vis spectrophotometer was used for absorption spectra measurements. AFM measurements were performed in air at room temperature using a Nanoscope III Multimode AFM (Digital Instruments, USA) operating in a tapping mode. The wall thickness of capsules was calculated by averaging the thickness of flat regions of at least 30 capsules.

Remote Release of Labeled Polymer from Microshells. A homemade laser setup equipped with a CW laser diode operating at 830 nm with intensities of up 90 mW was used according the earlier presented method.[26,42] The fluorescence of all capsules containing nonaggregated or aggregated gold particles that were irradiated once, but did not release their content, was irradiated a second time and observed again by LSCM. The fluorescence of irradiated capsules was also monitored 48 h after lasing to ensure that no capsules with nonaggregated nanoparticles, which after irradiation still had fluorescence, slowly released their content.

Temperature Simulation. In the simulations using the program Femlab (Comsol AB, USA), the heat capacity of water was taken as 4200 J/kg · K, heat conductivities of water and gold are 0.54 and 320 W/mK, respectively. The beam radius was taken at ~1 μm, and transmission through the objective[58] was taken at ~60%. Optical constants for gold were taken from the previously published work.[59]

Acknowledgment. We gratefully acknowledge H. Möhwald for constant support during research and fruitful discussions. We thank Rona Pitschke for TEM measurements, Anneliese Heilig for AFM measurements, and Heidi Zastrow for assistance with DLS, and the 6th FP EU projects STREP NMP3-CT-2005-516922 "SelectNANO" and PICT-2006-01365 (Max-Planck Society−Argentine SeCyt).

Supporting Information Available: Additional AFM images illustrating the surface roughness of microcapsules before and after thermal shrinking. Dynamic light scattering (DLS) illustrating the aggregation of gold nanoparticles after adding salt as a function of time. This material is available free of charge *via* the Internet at http://pubs.acs.org.

REFERENCES AND NOTES

1. Bruchez, M.; Moronne, M.; Gin, P.; Weiss, S.; Alivisatos, A. P. Semiconductor Nanocrystals as Fluorescent Biological Labels. *Science* **1998**, *281*, 2013–2016.
2. Kamat, P. V. Meeting the Clean Energy Demand: Nanostructure Architectures for Solar Energy Conversion. *J. Phys. Chem. C* **2007**, *111*, 2834–2860.
3. Jamieson, T.; Bakhshi, R.; Petrova, D.; Pocock, R.; Imani, M.; Seifalian, A. M. Biological Applications of Quantum Dots. *Biomaterials* **2007**, *28*, 4717–4732.
4. Bravo, J.; Zhai, L.; Wu, Z. Z.; Cohen, R. E.; Rubner, M. F. Transparent Superhydrophobic Films Based on Silica Nanoparticles. *Langmuir* **2007**, *23*, 7293–7298.
5. Hammond, P. T. Form and Function in Multilayer Assembly: New Applications at the Nanoscale. *Adv. Mater.* **2004**, *16*, 1271–1293.
6. Hua, F.; Cui, T. H.; Lvov, Y. Lithographic Approach to Pattern Self-Assembled Nanoparticle Multilayers. *Langmuir* **2002**, *18*, 6712–6715.
7. Whitesides, G. M.; Grzybowski, B. Self-Assembly at All Scales. *Science* **2002**, *295*, 2418–2421.
8. Sievers, T. K.; Kurth, D. G. Molecular Recognition in Functional Materials at Solid Interfaces. *Curr. Opin. Colloid Interface Sci.* **2008**, *13*, 86–95.
9. Link, S.; El-Sayed, M. A. Shape and Size Dependence of Radiative, Non-Radiative and Photothermal Properties of Gold Nanocrystals. *Int. Rev. Phys. Chem.* **2000**, *19*, 409–453.
10. Badia, A.; Cuccia, L.; Demers, L.; Morin, F.; Lennox, R. B. Structure and Dynamics in Alkanethiolate Monolayers Self-Assembled on Gold Nanoparticles: A DSC, FT-IR, and Deuterium NMR Study. *J. Am. Chem. Soc.* **1997**, *119*, 2682–2692.
11. Shon, Y. S.; Choo, H. Organic Reactions of Monolayer-Protected Metal Nanoparticles. *C.R. Chim.* **2003**, *6*, 1009–1018.
12. Caruso, F. Nanoengineering of Particle Surfaces. *Adv. Mater.* **2001**, *13*, 11–22.
13. Lu, C.; Mohwald, H.; Fery, A. Plasmon Resonance Tunable by Deaggregation of Gold Nanoparticles in Multilayers. *J. Phys. Chem. C* **2007**, *111*, 10082–10087.
14. Turkevich, J.; Stevenson, P. C.; Hillier, J. A Study of the Nucleation and Growth Processes in the Synthesis of Colloidal Gold. *Discuss. Faraday Soc.* **1951**, *11*, 55–75.
15. Mangeney, C.; Ferrage, F.; Aujard, I.; Marchi-Artzner, V.; Jullien, L.; Ouari, O.; Rekai, E. D.; Laschewsky, A.; Vikholm, I.; Sadowski, J. W. Synthesis and Properties of Water-Soluble Gold Colloids Covalently Derivatized with Neutral Polymer Monolayers. *J. Am. Chem. Soc.* **2002**, *124*, 5811–5821.
16. Richardson, H. H.; Hickman, Z. N.; Govorov, A. O.; Thomas, A. C.; Zhang, W.; Kordesch, M. E. Thermooptical Properties of Gold Nanoparticles Embedded in Ice: Characterization of Heat Generation and Melting. *Nano Lett.* **2006**, *6*, 783–788.
17. Donath, E.; Sukhorukov, G. B.; Caruso, F.; Davis, S. A.; Mohwald, H. Novel Hollow Polymer Shells by Colloid-Templated Assembly of Polyelectrolytes. *Angew. Chem., Int. Ed.* **1998**, *37*, 2202–2205.
18. Decher, G. Fuzzy Nanoassemblies: Toward Layered Polymeric Multicomposites. *Science* **1997**, *277*, 1232–1237.
19. Sukhorukov, G. B.; Rogach, A. L.; Garstka, M.; Springer, S.; Parak, W. J.; Munoz-Javier, A.; Kreft, O.; Skirtach, A. G.; Susha, A. S.; Ramaye, Y. Multifunctionalized Polymer Microcapsules: Novel Tools for Biological and Pharmacological Applications. *Small* **2007**, *3*, 944–955.
20. Lu, Z. H.; Shutava, T.; Sahiner, N.; John, V.; Lvov, Y. Photopolymerization of Acrylamide Derivatives in Polyelectrolyte Microcapsules. *Chem. Lett.* **2005**, *34*, 1536–1537.
21. Antipov, A. A.; Sukhorukov, G. B.; Leporatti, S.; Radtchenko, I. L.; Donath, E.; Mohwald, H. Polyelectrolyte Multilayer Capsule Permeability Control. *Colloids Surf., A* **2002**, *198*, 535–541.
22. Harris, J. J.; Bruening, M. L. Electrochemical and *In Situ* Ellipsometric Investigation of the Permeability and Stability of Layered Polyelectrolyte Films. *Langmuir* **2000**, *16*, 2006–2013.
23. Ibarz, G.; Dahne, L.; Donath, E.; Mohwald, H. Smart Micro- and Nanocontainers for Storage, Transport, and Release. *Adv. Mater.* **2001**, *13*, 1324–1327.
24. Farhat, T. R.; Schlenoff, J. B. Ion Transport and Equilibria in Polyelectrolyte Multilayers. *Langmuir* **2001**, *17*, 1184–1192.
25. Bedard, M.; Skirtach, A. G.; Sukhorukov, G. B. Optically Driven Encapsulation Using Novel Polymeric Hollow Shells Containing an Azobenzene. Polymer. *Macromol. Rapid Commun.* **2007**, *28*, 1517–1521.

26. Skirtach, A. G.; Javier, A. M.; Kreft, O.; Kohler, K.; Alberola, A. P.; Mohwald, H.; Parak, W. J.; Sukhorukov, G. B. Laser-Induced Release of Encapsulated Materials inside Living Cells. *Angew. Chem., Int. Ed.* **2006**, *45*, 4612–4617.
27. Radt, B.; Smith, T. A.; Caruso, F. Optically Addressable Nanostructured Capsules. *Adv. Mater.* **2004**, *16*, 2184–2189.
28. Borodina, T.; Markvicheva, E.; Kunizhev, S.; Moehwald, H.; Sukhorukov, G. B.; Kreft, O. Controlled Release of DNA from Self-Degrading Microcapsules. *Macromol. Rapid Commun.* **2007**, *28*, 1894–1899.
29. De Geest, B. G.; Dejugnat, C.; Prevot, M.; Sukhorukov, G. B.; Demeester, J.; De Smedt, S. C. Self-Rupturing and Hollow Microcapsules Prepared from Bio-Polyelectrolyte-Coated Microgels. *Adv. Funct. Mater.* **2007**, *17*, 531–537.
30. De Geest, B. G.; Skirtach, A. G.; Mamedov, A. A.; Antipov, A. A.; Kotov, N. A.; De Smedt, S. C.; Sukhorukov, G. B. Ultrasound-Triggered Release from Multilayered Capsules. *Small* **2007**, *3*, 804–808.
31. Shchukin, D. G.; Gorin, D. A.; Moehwald, H. Ultrasonically Induced Opening of Polyelectrolyte Microcontainers. *Langmuir* **2006**, *22*, 7400–7404.
32. Hartmann, L.; Bedard, M.; Borner, H. G.; Mohwald, H.; Sukhorukov, G. B.; Antonietti, M. CO_2-Switchable Oligoamine Patches Based on Amino Acids and Their Use to Build Polyelectrolyte Containers with Intelligent Gating. *Soft Matter* **2008**, *4*, 534–539.
33. El-Sayed, M. A. Small Is Different: Shape-, Size-, and Composition-Dependent Properties of Some Colloidal Semiconductor Nanocrystals. *Acc. Chem. Res.* **2004**, *37*, 326–333.
34. Perez-Juste, J.; Pastoriza-Santos, I.; Liz-Marzan, L. M.; Mulvaney, P. Gold Nanorods: Synthesis, Characterization and Applications. *Coord. Chem. Rev.* **2005**, *249*, 1870–1901.
35. Skirtach, A. G.; Karageorgiev, P.; De Geest, B. G.; Pazos-Perez, N.; Braun, D.; Sukhorukov, G. B. Nanorods as Wavelength-Selective Absorption Centers in the Visible and Near-Infrared Regions of the Electromagnetic Spectrum. *Adv. Mater.* **2008**, *20*, 506–510.
36. Kreibig, U.; Genzel, L. Optical-Absorption of Small Metallic Particles. *Surf. Sci.* **1985**, *156*, 678–700.
37. Norman, T. J.; Grant, C. D.; Magana, D.; Zhang, J. Z.; Liu, J.; Cao, D. L.; Bridges, F.; Van Buuren, A. Near Infrared Optical Absorption of Gold Nanoparticle Aggregates. *J. Phys. Chem. B* **2002**, *106*, 7005–7012.
38. Huang, X.; Qian, W.; El-Sayed, I. H.; El-Sayed, M. A. The Potential Use of the Enhanced Nonlinear Properties of Gold Nanospheres in Photothermal Cancer Therapy. *Lasers Surg. Med.* **2007**, *39*, 747–753.
39. Skirtach, A. G.; Dejugnat, C.; Braun, D.; Susha, A. S.; Rogach, A. L.; Sukhorukov, G. B. Nanoparticles Distribution Control by Polymers: Aggregates *versus* Nonaggregates. *J. Phys. Chem. C* **2007**, *111*, 555–564.
40. Ozin, G. A.; Arsenault, A. *Nanochemistry: A Chemical Approach to Nanomaterials*; Royal Chemistry Society: London, 2005.
41. Shipway, A. N.; Lahav, M.; Gabai, R.; Willner, I. Investigations into the Electrostatically Induced Aggregation of Au Nanoparticles. *Langmuir* **2000**, *16*, 8789–8795.
42. Skirtach, A. G.; Antipov, A. A.; Shchukin, D. G.; Sukhorukov, G. B. Remote Activation of Capsules Containing Ag Nanoparticles and Ir Dye by Laser Light. *Langmuir* **2004**, *20*, 6988–6992.
43. Dejugnat, C.; Kohler, K.; Dubois, M.; Sukhorukov, G. B.; Mohwald, H.; Zemb, T.; Guttmann, P. Membrane Densification of Heated Polyelectrolyte Multilayer Capsules Characterized by Soft X-Ray Microscopy. *Adv. Mater.* **2007**, *19*, 1331–1336.
44. Kohler, K.; Mohwald, H.; Sukhorukov, G. B. Thermal Behavior of Polyelectrolyte Multilayer Microcapsules: 2. Insight into Molecular Mechanisms for the PDADMAC/PSS System. *J. Phys. Chem. B* **2006**, *110*, 24002–24010.
45. Schonhoff, M.; Ball, V.; Bausch, A. R.; Dejugnat, C.; Delorme, N.; Glinel, K.; Klitzing, R. V.; Steitz, R. Hydration and Internal Properties of Polyelectrolyte Multilayers. *Colloids Surf., A* **2007**, *303*, 14–29.
46. Kohler, K.; Shchukin, D. G.; Mohwald, H.; Sukhorukov, G. B. Thermal Behavior of Polyelectrolyte Multilayer Microcapsules. 1. The Effect of Odd and Even Layer Number. *J. Phys. Chem. B* **2005**, *109*, 18250–18259.
47. Skirtach, A. G.; Dejugnat, C.; Braun, D.; Susha, A. S.; Rogach, A. L.; Parak, W. J.; Mohwald, H.; Sukhorukov, G. B. The Role of Metal Nanoparticles in Remote Release of Encapsulated Materials. *Nano Lett.* **2005**, *5*, 1371–1377.
48. Mueller, R.; Kohler, K.; Weinkamer, R.; Sukhorukov, G.; Fery, A. Melting of PDADMAC/PSS Capsules Investigated with AFM Force Spectroscopy. *Macromolecules* **2005**, *38*, 9766–9771.
49. M'Bareck, C. O.; Nguyen, Q. T.; Metayer, A.; Saiter, J. M.; Garda, M. R. Poly(Acrylic Acid) and Poly(Sodium Styrene Sulfonate) Compatibility by Fourier Transform Infrared and Differential Scanning Calorimetry. *Polymer* **2004**, *45*, 4181–4187.
50. Yeo, S. C.; Eisenberg, A. Physical Properties and Supermolecular Structure of Perfluorinated Ion-Containing (Nafion) Polymers. *J. Appl. Polym. Sci.* **1977**, *21*, 875–898.
51. Pitsillides, C. M.; Joe, E. K.; Wei, X.; Anderson, R. R.; Lin, C. P. Selective Cell Targeting with Light-Absorbing Microparticles and Nanoparticles. *Biophys. J.* **2003**, *84*, 4023–4032.
52. Govorov, A. O.; Zhang, W.; Skeini, T.; Richardson, H.; Lee, J.; Kotov, N. A. Gold Nanoparticle Ensembles as Heaters and Actuators: Melting and Collective Plasmon Resonances. *Nanoscale Res. Lett.* **2006**, *1*, 84–90.
53. Volkov, A. N.; Sevilla, C.; Zhigilei, L. V. Numerical Modeling of Short Pulse Laser Interaction with Au Nanoparticle Surrounded by Water. *Appl. Surf. Sci.* **2007**, *253*, 6394–6399.
54. Pissuwan, D.; Valenzuela, S. M.; Killingsworth, M. C.; Xu, X. D.; Cortie, M. B. Targeted Destruction of Murine Macrophage Cells with Bioconjugated Gold Nanorods. *J. Nanopart. Res.* **2007**, *9*, 1109–1124.
55. Jiang, C. Y.; Markutsya, S.; Pikus, Y.; Tsukruk, V. V. Freely Suspended Nanocomposite Membranes as Highly Sensitive Sensors. *Nat. Mater.* **2004**, *3*, 721–728.
56. Usta, O. B.; Alexeev, A.; Zhu, G.; Balazs, A. C. Modeling Microcapsules That Communicate through Nanoparticles to Undergo Self-Propelled Motion. *ACS Nano* **2008**, *2*, 471–476.
57. Shchukin, D. G.; Mohwald, H. Surface-Engineered Nanocontainers for Entrapment of Corrosion Inhibitors. *Adv. Funct. Mater.* **2007**, *17*, 1451–1458.
58. Neuman, K. C.; Chadd, E. H.; Liou, G. F.; Bergman, K.; Block, S. M. Characterization of Photodamage to *Escherichia coli* in Optical Traps. *Biophys. J.* **1999**, *77*, 2856–2863.
59. Johnson, P. B.; Christy, R. W. Optical-Constants of Noble-Metals. *Phys. Rev. B* **1972**, *6*, 4370–4379.